Published in final edited form as:
J Am Chem Soc. 2023 August 16; 145(32): 17656–17664. doi:10.1021/jacs.3c03639.

Using Data Science for Mechanistic Insights and Selectivity Predictions in a Non-Natural Biocatalytic Reaction

Hanna D. Clements,
Department of Chemistry, University of Utah, Salt Lake City, Utah 84112, United States

Autumn R. Flynn,
Department of Chemistry, University of Utah, Salt Lake City, Utah 84112, United States

Bryce T. Nicholls,
Department of Chemistry and Chemical Biology, Cornell University, Ithaca, New York 14853, United States

Daria Grosheva,
Department of Chemistry and Chemical Biology, Cornell University, Ithaca, New York 14853, United States

Sarah J. Lefave,
Department of Chemistry, University of Utah, Salt Lake City, Utah 84112, United States

Morgan T. Merriman,
Department of Chemistry, University of Utah, Salt Lake City, Utah 84112, United States

Todd K. Hyster,
Department of Chemistry and Chemical Biology, Cornell University, Ithaca, New York 14853, United States

Matthew S. Sigman
Department of Chemistry, University of Utah, Salt Lake City, Utah 84112, United States

Abstract

The study of non-natural biocatalytic transformations relies heavily on empirical methods, such as directed evolution, for identifying improved variants. Although exceptionally effective, this approach provides limited insight into the molecular mechanisms behind the transformations and necessitates multiple protein engineering campaigns for new reactants. To address this limitation, we disclose a strategy to explore the biocatalytic reaction space and garner insight into the molecular mechanisms driving enzymatic transformations. Specifically, we explored the selectivity of an “ene”-reductase, GluER-T36A, to create a data-driven toolset that explores reaction space and rationalizes the observed and predicted selectivities of substrate/mutant combinations. The

Corresponding Authors Todd K. Hyster – Department of Chemistry and Chemical Biology, Cornell University, Ithaca, New York 14853, United States, thyster@cornell.edu; **Matthew S. Sigman** – Department of Chemistry, University of Utah, Salt Lake City, Utah 84112, United States, sigman@chem.utah.edu.
Author Contributions
All authors have given approval to the final version of the manuscript.

The authors declare no competing financial interest.

resultant statistical models related structural features of the enzyme and substrate to selectivity and were used to effectively predict selectivity in reactions with out-of-sample substrates and mutants. Our approach provided a deeper understanding of enantioinduction by GluER-T36A and holds the potential to enhance the virtual screening of enzyme mutants.

Graphical Abstract

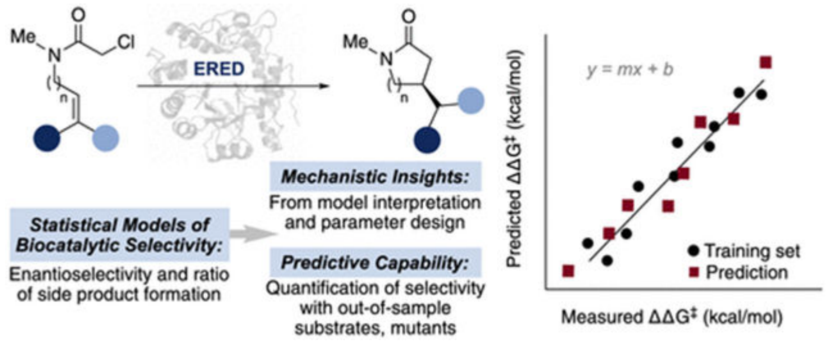
Me
N
O
Cl
n
ERED
Me
N
O
n
Statistical Models of Biocatalytic Selectivity:
Enantioselectivity and ratio of side product formation
Mechanistic Insights:
From model interpretation and parameter design
Predictive Capability:
Quantification of selectivity with out-of-sample substrates, mutants
y = mx + b
Predicted ΔΔG‡ (kcal/mol)
Measured ΔΔG‡ (kcal/mol)
● Training set
■ Prediction

INTRODUCTION

Enzymes play an expanding role as selective, efficient catalysts for biotechnology, biomedicine, biofuels, and industrial pharmacology.[1-4] The extension of enzymatic catalysis to non-native transformations generally relies on extensive screens of sequence space through protein engineering [e.g., directed evolution (DE)].[5,6] Advances in sequencing technologies and machine learning have enabled predictive modeling of biocatalyst reactivity. However, the widespread use of these methods is somewhat hindered due to the requirement for tremendous quantities of experimental data and the "black-box" nature of the algorithms used to guide optimization. Like DE, existing platforms for predictive biocatalysis do not necessarily capture or reveal the important mechanistic features of a given reaction and may not translate well to modified reactions (such as a similar reaction with a different substrate).

We were motivated to develop a strategy to simultaneously explore biocatalytic reaction space and gain insight into the molecular mechanisms behind non-native transformations. Specifically, we wanted to describe sequence space (enzyme mutants) and chemical space (substrate variants) in a quantitative manner using molecular descriptors and relate these descriptors to reaction outcomes, like enantioselectivity.[7] Unlike black-box methods for predictive biocatalysis, we postulated that simple statistical models constructed from smaller datasets could deliver not only predictive power but also valuable molecular-level insights into the origins of selective biocatalysis. We anticipated that attention to conformational dynamics and the use of information-rich molecular descriptors (of both enzyme and substrate) would result in models with greater interpretability and generalizability compared to existing methods.[8-12]

In this study, we demonstrate this approach in the context of non-native enantioselective photoenzymatic radical cyclization reactions catalyzed by "ene"-reductase (ERED) variants from *Gluconobacter oxydans* (GluER-T36A, Scheme 1).[13] We created a statistical toolset that explored GluER-T36A reaction space and rationalized the observed and predicted selectivities of previously untested substrate/mutant combinations. The emphasis on both substrate and enzyme diversity in model training allowed us to predict the selectivity of out-of-sample substrates in combination with new GluER-T36A variants. We demonstrated the adaptability of statistical models through the incorporation of additional experimental data and hypothesis-driven parameter advancement. The inclusion of multiple substrates in model training and development complemented existing in silico protein engineering methods (which often require separate datasets/analyses for each substrate).[14-16] Our results showcase the advantages of these tools in predicting and rationalizing the molecular interactions that drive enantioselective biocatalysis.

WORKFLOW DESIGN

A major challenge associated with building statistical models of biocatalyst selectivity was the availability of balanced training data. We, therefore, sought a system with which we could construct a training set containing a range of reaction outcomes to develop the statistical modeling workflow. EREDs were selected as a model biocatalytic framework as they have been reliably utilized in a range of non-native enantioselective reactions.[17-21] GluER-T36A is a selective catalyst for the photoenzymatic cyclization of many α-chloroamides (Scheme 1); however, a number of substrates had to be paired with homologous EREDs to achieve high enantioselectivity in the initial report.[13] Although effective in this instance, the general practice of shifting enzyme frameworks can lead to unexpected results (i.e., enantiodivergent transformations or byproducts) and introduce challenges including reoptimization of expression and reaction conditions.[20,21] To circumvent these challenges, we sought to develop explanatory statistical models. These models would relate structural features of a small but diverse sample of GluER-T36A variants and α-chloroamide substrates to selectivity and draw from all training data, including poorly performing substrate/mutant combinations. Notably, this strategy avoids the requirement for screening thousands of mutants and cyclic evaluation of mutant libraries to expand the reaction scope.

In this context, we designed a focused training set with diversity in both substrate characteristics and enzyme mutations. The transformation of substrates **1a–4a** (Scheme 1) encompass three different cyclization modes (**1a**: 5-*endo*-trig, **2a**, **3a**: 5-*exo*-trig, and **4a**: 6-*exo*-trig), varying electronic properties (as in **2a** and **3a**), and alkene substitution patterns (**1a** vs **2a–4a**). Informed by previous studies on GluER-T36A, we identified five residues within the GluER-T36A active site for mutation: W66, Y177, Q232, F269, and Y343. Mutations at these sites were shown to retain activity while affecting selectivity in the cyclization, although the mechanism of selectivity modulation was not well-understood. We preformed site-directed mutagenesis to introduce residues W, F, D, L, or A at each of the five sites as these mutations would sample a range of residue properties. Substrates **1a–4a** were subjected to reactions with each expressible mutant, resulting in a total of 50 datapoints to use in model training and selection. A full table of substrate/enzyme combinations and the resultant ee's is included in Table S1.

We next considered strategies to computationally characterize both enzyme and ligand (substrate and product) structures for descriptor extraction. We have previously described methods to characterize small-molecule catalysts and compute chemical descriptors by pairing molecular mechanics (MM)-based structural analysis with density functional theory (DFT) calculations.[22,23] However, the shift to biocatalytic platforms presents several unique challenges. The size and elaborate dynamics of enzymes have necessitated bespoke computational strategies to study enzyme/ligand complexes [EL]; however, many of these are best suited for in-depth analysis of one or a few [EL] pairs due to their operational complexity and resource demands.[24,25] We therefore sought workflows that would account for the dynamic nature of biocatalysts while also introducing scalability and consideration of ligand interactions.

We identified two complementary conformational search platforms: molecular dynamics (MD) and induced fit docking (IFD) (Figure 1A). Typical MD simulations allow for flexibility in the entire enzyme; however, they also require substantial computational resources to sample enzyme conformations. To increase the scalability of the MD workflow, we utilized an enhanced sampling method, accelerated MD (aMD). This method artificially lowers the kinetic barriers in MD simulations through systematic perturbation of the potential energy surface.[26,27] We employed aMD to sample a larger number of GluER conformers without lengthening the MD simulation. Another step to reduce the computational cost of the aMD conformational search was to pair the enzyme structures with conformational ensembles of the free ligand (both substrate and product structures) from MM/DFT. The separate assembly of enzyme and ligand structures in the aMD sampling approach makes it easily applicable to large enzyme/ligand matrices and has potential for virtual screening (vide infra).

As an alternative to the aMD conformer search, which requires supercomputing resources and expert knowledge, we directly probed the [EL] conformers with IFD. IFD is a MM-based docking protocol that approximates the docking pose of a ligand and the concomitant repositioning of nearby enzyme residues.[28-30] Previously, we applied IFD to engineer a more promiscuous variant of the prenyltransferase, NotF.[31] Using the mechanistic insights gained from IFD simulations, we identified a NotF mutation that allowed the prenyltransferase to accept a more sterically demanding substrate. Here, we have expanded the use of IFD as a tool for collecting [EL] conformational ensembles. This conformational search method scales with the number of [EL] complexes, but unlike the aMD platform, it offers the advantage of directly probing the interactions between the small molecule and biocatalyst.

Upon acquisition of the enzyme and ligand conformational ensembles with either aMD or IFD, chemical descriptors were computed, automatically extracted, and curated for the ligands as well as for individual residues in the active site (Figure 1B). These descriptors included electronic (e.g., NBO charges),[32] steric (e.g., sterimol values),[33] and dynamic descriptors, which measure the topographical properties of a collection of conformers [e.g., dynamic surface area (DSA)].[34] Although this initial parameterization strategy neglected the interactions between protein residues, we hypothesized that representing the active site by its individual residues in this manner could reveal the residues that have the most influence on reaction enantioselectivity (vide infra).

Finally, descriptors were regressed against the experimentally collected dataset (70:30 split of training and validation set data points, enantioselectivity expressed as $\Delta\Delta G^{\ddagger}$, which is proportional to the log of the measured enantiomeric ratio) using a forward-stepwise multivariate linear regression (MLR) algorithm, which resulted in numerous candidate models for each conformational search platform (Figure 1C).[22]

RESULTS AND DISCUSSION

From the candidate models, we identified a representative high-performing aMD statistical model (Figure 2A) that had a training R^2 of 0.82 and a mean absolute error (MAE) in $\Delta\Delta G^{\ddagger}$ of 0.19 kcal/mol, indicating a good correlation between the measured and predicted values of the training set. The validation R^2 is the correlation between measured and predicted values for the validation set (the partition of data that was withheld from model training); the aMD model had a validation R^2 of 0.73 and a corresponding validation MAE = 0.19 kcal/mol. As for the parameters in the aMD model, $\Delta\mathrm{NBO}_{\mathrm{pdt},\beta\text{-C}}$ is the difference in the maximum and minimum NBO charge on the product β-carbon; ΔSterimol L_{sub} is the difference in the maximum and minimum substituent length values (flexibility) of substrate structures. Residue $66_{\Delta\mathrm{Sterimol}\ L}$ is the difference in the maximum and minimum residue length values (flexibility) of residue 66. Residue $100_{\Delta\mathrm{Angle}\ 1}$ and Residue $342_{\Delta\mathrm{Angle}\ 3}$ are the difference in the maximum and minimum of these angles (see Supporting Information). Residue $172_{\mathrm{Sterimol}\ L,\mathrm{max}}$ is the maximum length of residue 172.

The selected IFD statistical model (Figure 2B) demonstrated a training R^2 of 0.83 with a MAE of 0.18 kcal/mol, suggesting that the aMD and IFD models performed similarly in their capability to describe the data in the training set. The IFD model had a validation R^2 of 0.57 and a corresponding validation MAE of 0.29 kcal/mol. Identification of statistical models from both IFD and aMD workflows validated our hypothesis that molecular features of enzyme residues and ligands can describe the outcome of a biocatalytic reaction. $\mathrm{NBO}_{\mathrm{pdt,carbonyl\ O}}$ is the NBO charge of the carbonyl oxygen on product structures. $\mathrm{NBO}_{\mathrm{pdt},\beta\text{-H,min}}$ is the minimum NBO charge of the hydrogen bound to the β-carbon in product structures. Residue $100_{\mathrm{pdt,Sterimol\ B5}}$ is the maximum width of residue 100 from product-docked enzyme structures. Residue $269_{\mathrm{sub,Sterimol\ B5GS}}$ is the GScore (docking-score) weighted maximum width of residue 269 from the substrate-docked enzyme structures. Residue $100_{\mathrm{pdt,DSA}}$ and Residue $172_{\mathrm{pdt,DSA}}$ are the DSAs of residues 100 and 172 from product-docked enzyme structures, respectively. Residue $343_{\mathrm{sub},\Delta\mathrm{Sterimol}\ L}$ is the difference in the maximum and minimum length (flexibility) of residue 343 from substrate-docked enzyme structures.

Unlike established procedures to predict biocatalyst selectivity, the statistical models presented herein possess the ability to evaluate substrates that were not included in model training. We, therefore, used both aMD and IFD statistical models to predict the performance of various GluER-T36A mutants with two new substrates: **5a** and **6a** (Figure 2C). These were selected to incorporate substrate characteristics that were not represented in the training set, including an alkyl-substituted example (**5a**) and a different cyclization mode (**6a**, 7-*exo*-trig). For the aMD model, **5a** and **6a** conformers were collected and combined with existing enzyme trajectories, and for IFD, the relevant [EL] poses were generated. The enantioselectivities of **5a** and **6a** with each GluER-T36A variant were predicted using the statistical models from Figure 2a,b. Gratifyingly, in the experimental evaluation of these combinations, the models performed generally well in predicting the selectivity of GluER-T36A variants with the out-of-sample substrates. The aMD model was somewhat more successful, with a MAE of 0.38 kcal/mol for the out-of-sample substrate predictions, compared to a MAE of 0.48 kcal/mol for the IFD model.

In addition to the competing diastereomeric transition states in the desired cyclization, a hydrodehalogenation pathway can also interfere with the cyclization process through H-atom transfer (HAT) to the putative α-acyl radical (as shown in Figure 3). The relative ratio of cyclization to HAT appeared to be primarily substrate-dependent, with the lowest levels of HAT detected in the 5-*exo*-trig cyclization of aryl substrates **2a** and **3a**. Despite the strong substrate dependence, some GluER-T36A variants modulate preference for the HAT pathway (Table S1), and we sought to capture GluER-T36A chemoselectivity through a separate statistical model.

We found that regressing with the previously collected IFD descriptor set resulted in the best statistical model (training and validation R^2 of 0.82 and 0.70, respectively, Figure 3A). As expected from the observed substrate dependence, the HAT model primarily featured ligand descriptors: $\mathrm{NBO}_{\mathrm{pdt\ carbonyl\ C,GS}}$ is the docking score-weighted NBO of the carbon atom of the product carbonyl. $\mathrm{NBO}_{\mathrm{pdt},\beta\text{-}\mathrm{H,GS}}$ is the docking score-weighted NBO of the hydrogen atom bound to the β-carbon in product structures. Sterimol $L_{\mathrm{pdt,min}}$ describes the minimum length of the lactam substituent off the β-carbon in product structures. Simply put, the ligand features suggested that the electronic nature of the stereocenter formed in the cyclization and size of the lactam substituent when bound to the active site are largely responsible for the observed cyclization/HAT rate differences. Additionally, catalyst identity can modulate preference for the cyclization pathway, namely, through the repositioning of residue 269 (Residue $269_{\mathrm{Sterimol\ B5sub,GS}}$ is the docking score-weighted maximum width of residue 269, generated from substrate-docked enzyme structures).

As an external validation of this model, we predicted the cyclization to HAT ratio of substrate **6a** with a suite of GluER-T36A mutations. IFD appears to be particularly well suited for this analysis as it explicitly sampled ligand position for each GluER-T36A variant.

We next turned our attention to virtual screening GluER-T36A variants to predict how mutations impact selectivity in cyclization. We aimed to predict selectivity with multiple substrates and therefore utilized the aMD workflow, which scales with the number of enzyme variants screened rather than with the number of [EL] complexes. We took a rather ambitious tact by exploring a virtual library of GluER-T36A double and triple mutants even though only single mutants were initially used in the training data. The statistical models were used to predict the selectivity of each variant with the model substrate **2a** and an alkyl substrate **5a**. We selected only mutants that extrapolated beyond the enantioselectivities observed in the training data. The putative hits were expressed, but unfortunately, subjecting them to the reaction conditions resulted in little or no enantioenrichment of products **2b** and **5b** and other substrates (Table S2). This disappointing result suggested that poor extrapolation of the aMD model to new enzyme mutants was a result of the relatively small number of GluER-T36A single mutants used in model training and/or because the quantitative descriptors that were used to characterize the enzymes did not account for interactions between residues.

To address these challenges, we interrogated the initial statistical models and developed a mechanistic hypothesis that enabled us to create reaction-specific descriptors (Figure 4). The aMD and IFD models showed a correlation between GluER-T36A selectivity and the relative positioning of aromatic residues 66, 100, and 177, consistent with studies of homologous EREDs.[35-38] Features describing residue 100 conveyed that increased flexibility led to decreased enantioselectivity. Similarly, the negative coefficient associated with residue 66 (Residue $66_{\Delta\text{-Sterimol } L}$) in the aMD model indicated that the dynamic behavior of this residue contributes to enhanced selectivity in the cyclization. Inspection of the aMD conformers revealed that W100 is involved in a network of competitive non-covalent interactions with flanking residues 66 and 177, where a strong (rigid) integration between residues 100 and 177 enables residue 66 to have a wider range of motion. Interestingly, IFD revealed significant repositioning of residue 66 upon substrate **6a** binding, suggesting that mobility of this residue is essential for proper substrate orientation (Figure 4A, right). We leveraged this insight to design new enzyme descriptors, which were focused on interactions between adjacent residues to better represent the contacts between residues 66, 100, and 177 (Figure 5). The DSA method was expanded to calculate the DSA of a group of proximal residues. For example, conformers of residues 66 and 100 were enclosed in a hypothetical surface, then the surface area and volume of the cluster were computed to determine the cDSA and cDV, respectively (Figure 5A). To further probe the interactions between residues 66, 100, and 177, R-group centroids were measured to describe inter-residue distances (IRD, Figure 5B).

Having characterized the interactions between residues 66, 100, and 177, our focus then shifted to residues 172, 175, and 177. Both initial models found that the conformation of H172 is crucial for reaction selectivity. The aMD parameter for H172 measures its most extended conformation in each GluER-T36A variant; the aMD structures show that when H172 is extended, nearby residues N175 and Y177 are displaced, creating a distinct binding pocket (depicted as yellow spheres in Figure 4B, right). We suggest the open binding site observed in GluER-T36A-F269L allows for facile substrate binding and reduces the risk of substrate dissociation or rotation. Conversely, when H172 is retracted, as in the case of GluER-T36A-Y177W, the binding pocket is occluded by nearby residues, leading to reduced enantioselectivity.[39] To interrogate this hypothesis, the cDSA, cDV, and associated IRDs for residue 172 and neighboring residues 175 and 177 were added to our enzyme descriptor set.

In addition to investigating the residue–residue interactions that were informed by our statistical models, we aimed to better understand the role of overall dynamics and flexibility in reaction enantioselectivity through feature development. To achieve this, we measured a residue’s flexibility over the course of the entire aMD trajectory rather than just within the clustered conformational ensemble. The frames from each aMD trajectory were aligned, and the RMSD of the backbone atoms was measured for active site residues. Similarly, R-group flexibility was measured using the RMSD of side-chain nonhydrogen atoms (Figure 5C). A complete list of residues, cDSA, IRD, and RMSD measurements is available in Table S4.

PREDICTING SELECTIVITY OF NEW GLUER-T36A MUTANTS

The newly designed enzyme descriptors (Figure 5) and additional experimental data from the previous virtual screen (Table S2) were merged with the initial dataset for a subsequent round of statistical modeling. In addition to training and validation set statistics (R^2 and MAE), a simulated virtual screening was used to identify three similar candidate models for prospective virtual screening (full details are available in the Supporting Information). To validate the models, a library of untested GluER-T36A variants was generated in silico for a virtual screen with substrates **2a** and **5a**. Using the aMD workflow, conformational ensembles for 39 single-point mutants at positions 66, 269, and 343 (sites at which mutations had previously preserved activity while affecting selectivity in the photoenzymatic cyclization) were collected, and the relevant parameters for the models were assembled. Unfortunately, the virtual screen did not suggest that any of these mutants would result in increased enantioenrichment in products **2b** and **5b** compared to previously tested GluER-T36A variants. Nonetheless, eight mutants, which were predicted to have a range of experimental outcomes, were selected from the in silico library for expression to validate the statistical model. Additional details of the virtual screening, mutant selection, and model comparison are available in the Supporting Information. The MLR models performed generally well in predicting how the new GluER-T36A mutants affected the enantioselectivity for products **2b** and **5b**. The best MLR model predicted the mutant performance with a MAE of 0.31 kcal/mol, and quantitative prediction of performance (within a 99% confidence interval computed from model bootstrapping with 1000 subsamples) was achieved for 6/14 of the reactions with out-of-sample enzymes (Figure 6). This performance was substantially better than the predictions from a regularized model trained on the complete feature set (Figure S6).

The updated statistical model is similar to the initial aMD model in several respects, including the use of a conserved electronic descriptor (the range in the charge on the carbonyl- or β-C in the lactam product, $\Delta\text{NBO}_{\text{pdt,carbonyl-C}}$ or $\Delta\text{NBO}_{\text{pdt},\beta\text{-C}}$, respectively) and a substrate steric descriptor (Sterimol $\text{B5}_{\text{sub,min}}$ or ΔSterimol L_{sub}). Additionally, the models have similar enzyme parameters describing the flexibility of residue 66 (Residue $66_{\text{Sterimol B5,max}}$ and Residue $66_{\Delta\text{Sterimol } L}$). The updated model also includes residue-specific descriptors for the maximum backbone angle of residue 175 (Residue $175_{\text{Angle 1,max}}$), and the minimum backbone dihedral angles of residues 261 and 269 (Residue $261_{\text{dihedral,min}}$ and Residue $269_{\text{dihedral,min}}$, respectively).

As described in the previous section, we postulated that when residue 100 preferentially interacts with residue 177, it disengages interactions with residue 66, enabling the necessary flexibility of that residue for proper repositioning upon substrate binding. Further supporting this hypothesis, the IRD parameter (IRD residues 100–177) in the updated model indicates that selectivity declines when residue 100 is far from residue 177. The new enzyme descriptors, informed from our mechanistic analysis of the initial statistical models, strengthened our understanding of GluER-T36A selectivity and enabled us to predict the effect of untested GluER-T36A mutations.

The GluER-T36A-Y343C variant was predicted to be most selective for both **2a** and **5a**, but the measured enantioselectivity was significantly over-predicted. To probe the origin of this apparent outlier, we compared the aMD conformers for GluER-T36A and the Y343C mutant, which revealed that adjacent residue W342 interacts with F269, a residue located on a loop adjacent to the active site. The loop is positioned to form a “lid” over the active site, and inspection of the GluER-T36A-Y343C conformational ensemble depicted a key difference from other GluER-T36A variants evaluated. The F269 loop is substantially displaced as a result of the Y343C mutation (Figure 7). Interestingly, similar mutations (Y343M) and even mutations to the loop (F269C, M, and R) do not result in comparable disorder. This structural anomaly supports that this prediction is likely an outlier as flexibility at this position is beneficial for enantioselectivity, but importantly, these models were not trained to recognize that major disruptions to the F269 loop are detrimental.

IFD experiments did not show alterations to the loop region as a result of the Y343 mutant, but an interesting change in the geometry of the bound lactam products was observed. These observations are seeding future studies to explore global [EL] features.

CONCLUSIONS

In summary, we have developed predictive tools to evaluate enzyme mutant performance on a non-native reaction while gaining a deeper mechanistic understanding. We identified two complementary conformational search platforms, aMD and IFD, to computationally characterize both enzyme and ligand structures for descriptor extraction and demonstrated how descriptors can be informed by evolving mechanistic hypothesis.

By utilizing a small, representative training set that encompasses a range of reaction outputs, we developed robust statistical models relating GluER-T36A structural features to function in an enantioselective cyclization. Although the focused training set used in this study was insufficient to predict reaction yields, we were able to construct a statistical model to capture the effects of the ligand and GluER-T36A variant on preference for a competing HAT pathway. These models allowed us to quantitatively predict the performance of out-of-sample substrates and substrate/mutant combinations, with a particular emphasis on substrate scope. Interpretation of the predictive model increased our understanding of the enantioinduction imparted by GluER-T36A, which complements contemporary approaches.[40,41] Future applications of this workflow will include the enhancement of enzymatic descriptors and virtual screening of enzyme mutants for reaction engineering.

Supplementary Material

Refer to Web version on PubMed Central for supplementary material.

ACKNOWLEDGMENTS

The computational portion of this work was supported by the Center for High Performance Computing (CHPC) at the University of Utah. This research was supported by the National Institutes of Health National Institute of

General Medical Sciences (R01 GM127703 to T.K.H. and R35 GM136271 to M.S.S.). This research made use of the Cornell University NMR Facility, which is supported, in part, by the NSF through MRI Award CHE-1531632. D.G. was supported by a Swiss National Science Foundation Early Postdoc Mobility Fellowship (no number).

REFERENCES

(1). Huffman MA; Fryszkowska A; Alvizo O; Borra-Garske M; Campos KR; Canada KA; Devine PN; Duan D; Forstater JH; Grosser ST; Halsey HM; Hughes GJ; Jo J; Joyce LA; Kolev JN; Liang J; Maloney KM; Mann BF; Marshall NM; McLaughlin M; Moore JC; Murphy GS; Nawrat CC; Nazor J; Novick S; Patel NR; Rodriguez-Granillo A; Robaire SA; Sherer EC; Truppo MD; Whittaker AM; Verma D; Xiao L; Xu Y; Yang H Design of an in Vitro Biocatalytic Cascade for the Manufacture of Islatravir. Science 2019, 366, 1255–1259. [PubMed: 31806816]

(2). Meghwanshi GK; Kaur N; Verma S; Dabi NK; Vashishtha A; Charan PD; Purohit P; Bhandari HS; Bhojak N; Kumar R Enzymes for Pharmaceutical and Therapeutic Applications. Biotechnol. Appl. Biochem 2020, 67, 586–601. [PubMed: 32248597]

(3). Duza MB; Mastan SA Microbial Enzymes and Their Applications—a Review. Indo Am. J. Pharm. Res 2013, 3, 651–657.

(4). Akyilmaz E; Yorganci E; Asav E Do Copper Ions Activate Tyrosinase Enzyme? A Biosensor Model for the Solution. Bioelectrochemistry 2010, 78, 155–160. [PubMed: 19840905]

(5). Arnold FH Directed Evolution: Bringing New Chemistry to Life. Angew. Chem., Int. Ed 2018, 57, 4143–4148.

(6). Bornscheuer UT; Huisman GW; Kazlauskas RJ; Lutz S; Moore JC; Robins K Engineering the Third Wave of Biocatalysis. Nature 2012, 485, 185–194. [PubMed: 22575958]

(7). Crawford JM; Kingston C; Toste FD; Sigman MS Data Science Meets Physical Organic Chemistry. Acc. Chem. Res 2021, 54, 3136–3148.

(8). Fox RJ; Davis SC; Mundorff EC; Newman LM; Gavrilovic V; Ma SK; Chung LM; Ching C; Tam S; Muley S; Grate J; Gruber J; Whitman JC; Sheldon RA; Huisman GW Improving Catalytic Function by ProSAR-Driven Enzyme Evolution. Nat. Biotechnol 2007, 25, 338–344. [PubMed: 17322872]

(9). Niu J; Yu G Molecular Structural Characteristics Governing Biocatalytic Chlorination of PAHs by Chloroperoxidase from Caldariomyces Fumago. SAR QSAR Environ. Res 2004, 15, 159–167. [PubMed: 15293544]

(10). Wittmann BJ; Johnston KE; Wu Z; Arnold FH Advances in Machine Learning for Directed Evolution. Curr. Opin. Struct. Biol 2021, 69, 11–18. [PubMed: 33647531]

(11). Robinson SL; Smith MD; Richman JE; Aukema KG; Wackett LP Machine Learning-Based Prediction of Activity and Substrate Specificity for OleA Enzymes in the Thiolase Superfamily. Synth. Biol 2020, 5, ysaa004.

(12). Goldman S; Das R; Yang KK; Coley CW Machine Learning Modeling of Family Wide Enzyme-Substrate Specificity Screens. PLoS Comput. Biol 2022, 18, No. e1009853. [PubMed: 35143485]

(13). Biegasiewicz KF; Cooper SJ; Gao X; Oblinsky DG; Kim JH; Garfinkle SE; Joyce LA; Sandoval BA; Scholes GD; Hyster TK Photoexcitation of Flavoenzymes Enables a Stereoselective Radical Cyclization. Science 2019, 364, 1166–1169. [PubMed: 31221855]

(14). Yang KK; Wu Z; Arnold FH Machine-Learning-Guided Directed Evolution for Protein Engineering. Nat. Methods 2019, 16, 687–694. [PubMed: 31308553]

(15). Wu Z; Jennifer Kan SB; Lewis RD; Wittmann BJ; Arnold FH Erratum: Machine Learning-Assisted Directed Protein Evolution with Combinatorial Libraries (Proceedings of the National Academy of Sciences of the United States of America (2019) 116 (8852–8858) DOI: 10.1073/Pnas.1901979116). Proc. Natl.Acad. Sci. U.S.A 2019, 117, 788–789. [PubMed: 31888994]

(16). Cadet F; Fontaine N; Li G; Sanchis J; Ng Fuk Chong M; Pandjaitan R; Vetrivel I; Offmann B; Reetz MT A Machine Learning Approach for Reliable Prediction of Amino Acid Interactions and Its Application in the Directed Evolution of Enantioselective Enzymes. Sci. Rep 2018, 8, 16757. [PubMed: 30425279]

(17). Clayman PD; Hyster TK Photoenzymatic Generation of Unstabilized Alkyl Radicals: An Asymmetric Reductive Cyclization. J. Am. Chem. Soc 2020, 142, 15673–15677. [PubMed: 32857506]

(18). Gao X; Turek-Herman JR; Choi YJ; Cohen RD; Hyster TK Photoenzymatic Synthesis of α-Tertiary Amines by Engineered Flavin-Dependent "Ene"-Reductases. J. Am. Chem. Soc 2021, 143, 19643–19647. [PubMed: 34784482]

(19). Laguerre N; Riehl PS; Oblinsky DG; Emmanuel MA; Black MJ; Scholes GD; Hyster TK Radical Termination via β-Scission Enables Photoenzymatic Allylic Alkylation Using "Ene"-Reductases. ACS Catal. 2022, 12, 9801–9805. [PubMed: 37859751]

(20). Page CG; Cooper SJ; Dehovitz JS; Oblinsky DG; Biegasiewicz KF; Antropow AH; Armbrust KW; Ellis JM; Hamann LG; Horn EJ; Oberg KM; Scholes GD; Hyster TK Quaternary Charge-Transfer Complex Enables Photoenzymatic Intermolecular Hydroalkylation of Olefins. J. Am. Chem. Soc 2021, 143, 97–102. [PubMed: 33369395]

(21). Huang X; Wang B; Wang Y; Jiang G; Feng J; Zhao H Photoenzymatic Enantioselective Intermolecular Radical Hydroalkylation. Nature 2020, 584, 69–74. [PubMed: 32512577]

(22). Santiago CB; Guo JY; Sigman MS Predictive and Mechanistic Multivariate Linear Regression Models for Reaction Development. Chem. Sci 2018, 9, 2398–2412. [PubMed: 29719711]

(23). Sigman MS; Harper KC; Bess EN; Milo A The Development of Multidimensional Analysis Tools for Asymmetric Catalysis and Beyond. Acc. Chem. Res 2016, 49, 1292–1301. [PubMed: 27220055]

(24). Ahmadi S; Barrios Herrera L; Chehelamirani M; Hostaš J; Jalife S; Salahub DR Multiscale Modeling of Enzymes: QM-Cluster, QM/MM, and QM/MM/MD: A Tutorial Review. Int. J. Quantum Chem 2018, 118, No. e25558.

(25). van der Kamp MW; Mulholland AJ Combined Quantum Mechanics/Molecular Mechanics (QM/MM) Methods in Computational Enzymology. Biochemistry 2013, 52, 2708–2728. [PubMed: 23557014]

(26). Case DA; Betz RM; Cerutti DS; Cheatham TE III; Darden TA; Duke RE; Giese TJ; Gohlke H; Goetz AW; Homeyer N AMBER 2016 Reference Manual; University of California: San Francisco, CA, USA, 2016; 1–923.

(27). Hamelberg D; Mongan J; McCammon JA Accelerated Molecular Dynamics: A Promising and Efficient Simulation Method for Biomolecules. J. Chem. Phys 2004, 120, 11919–11929. [PubMed: 15268227]

(28). Sherman W; Day T; Jacobson MP; Friesner RA; Farid R Novel Procedure for Modeling Ligand/Receptor Induced Fit Effects. J. Med. Chem 2006, 49, 534–553. [PubMed: 16420040]

(29). Sherman W; Beard HS; Farid R Use of an Induced Fit Receptor Structure in Virtual Screening. Chem. Biol. Drug Des 2006, 67, 83–84. [PubMed: 16492153]

(30). Farid R; Day T; Friesner RA; Pearlstein RA New Insights about HERG Blockade Obtained from Protein Modeling, Potential Energy Mapping, and Docking Studies. Bioorg. Med. Chem 2006, 14, 3160–3173. [PubMed: 16413785]

(31). Kelly SP; Shende VV; Flynn AR; Dan Q; Ye Y; Smith JL; Tsukamoto S; Sigman MS; Sherman DH Data Science-Driven Analysis of Substrate-Permissive Diketopiperazine Reverse Prenyltransferase NotF: Applications in Protein Engineering and Cascade Biocatalytic Synthesis of (−)-Eurotiumin A. J. Am. Chem. Soc 2022, 144, 19326–19336. [PubMed: 36223664]

(32). Glendening ED; Landis CR; Weinhold F NBO 6.0: Natural Bond Orbital Analysis Program. J. Comput. Chem 2013, 34, 1429–1437. [PubMed: 23483590]

(33). Verloop A. Drug Design; Ariens EJ, Ed.; Academic Press: New York, 1976; Vol. III.

(34). Guo JY; Minko Y; Santiago CB; Sigman MS Developing Comprehensive Computational Parameter Sets to Describe the Performance of Pyridine-Oxazoline and Related Ligands. ACS Catal. 2017, 7, 4144–4151.

(35). Kress N; Rapp J; Hauer B Enantioselective Reduction of Citral Isomers in NCR Ene Reductase: Analysis of an Active-Site Mutant Library. ChemBioChem 2017, 18, 717–720. [PubMed: 28176464]

(36). Ying X; Yu S; Huang M; Wei R; Meng S; Cheng F; Yu M; Ying M; Zhao M; Wang Z Engineering the Enantioselectivity of Yeast Old Yellow Enzyme Oye2Y in Asymmetric Reduction of (E/Z)-Citral to (R)-Citronellal. Molecules 2019, 24, 1057. [PubMed: 30889828]

(37). Pompeu YA; Sullivan B; Stewart JD X-Ray Crystallography Reveals How Subtle Changes Control the Orientation of Substrate Binding in an Alkene Reductase. ACS Catal. 2013, 3, 2376–2390.

(38). Padhi SK; Bougioukou DJ; Stewart JD Site-Saturation Mutagenesis of Tryptophan 116 of Saccharomyces Pastorianus Old Yellow Enzyme Uncovers Stereocomplementary Variants. J. Am. Chem. Soc 2009, 131, 3271–3280. [PubMed: 19226127]

(39). Richter N; Gröger H; Hummel W Asymmetric Reduction of Activated Alkenes Using an Enoate Reductase from Gluconobacter Oxydans. Appl. Microbiol. Biotechnol 2011, 89, 79–89. [PubMed: 20717668]

(40). Meng Q; Ramírez-Palacios C; Capra N; Hooghwinkel ME; Thallmair S; Rozeboom HJ; Thunnissen AMWH; Wijma HJ; Marrink SJ; Janssen DB Computational Redesign of an ω-Transaminase FromPseudomonas Jesseniifor Asymmetric Synthesis of Enantiopure Bulky Amines. ACS Catal. 2021, 11, 10733–10747. [PubMed: 34504735]

(41). Garcia-Borràs M; Kan SBJ; Lewis RD; Tang A; Jimenez-Osés G; Arnold FH; Houk KN Origin and Control of Chemoselectivity in Cytochrome c Catalyzed Carbene Transfer into Si—H and N—H Bonds. J. Am. Chem. Soc 2021, 143, 7114–7123. [PubMed: 33909977]

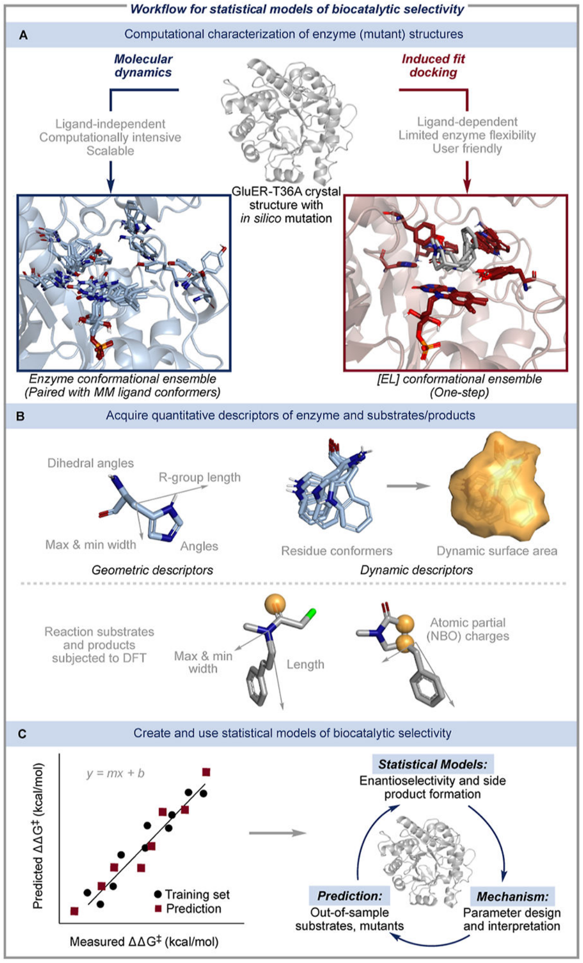
Workflow for statistical models of biocatalytic selectivity
A
Computational characterization of enzyme (mutant) structures
Molecular dynamics
Ligand-independent
Computationally intensive
Scalable
GluER-T36A crystal structure with *in silico* mutation
Induced fit docking
Ligand-dependent
Limited enzyme flexibility
User friendly
Enzyme conformational ensemble
(Paired with MM ligand conformers)
[EL] conformational ensemble
(One-step)
B
Acquire quantitative descriptors of enzyme and substrates/products
Dihedral angles
R-group length
Max & min width
Angles
Geometric descriptors
Residue conformers
Dynamic surface area
Dynamic descriptors
Reaction substrates and products subjected to DFT
Max & min width
Length
Atomic partial (NBO) charges
C
Create and use statistical models of biocatalytic selectivity
y = mx + b
Predicted ΔΔG‡ (kcal/mol)
Measured ΔΔG‡ (kcal/mol)
● Training set
■ Prediction
Statistical Models:
Enantioselectivity and side product formation
Prediction:
Out-of-sample substrates, mutants
Mechanism:
Parameter design and interpretation

Figure 1.

Workflow to develop statistical models of biocatalytic reaction performance. (A) Two complementary approaches, aMD and IFD, were used to generate enzyme conformers from a GluER-T36A crystal structure (PDB ID: 6MYW) after introducing the desired mutation in silico. (B) Enzyme features were quantified using a residue-based approach. Geometric descriptors include the length, width, and backbone angles of each residue conformer and the fluctuations of these measurements. Dynamic descriptors were measured by overlaying a residue conformational ensemble, encapsulating it in a fictitious surface, and measuring the resulting surface area and volume. Ligands were subjected to both a geometric analysis and DFT calculations to acquire electronic descriptors, including the natural bond orbital (NBO) charges of atoms indicated by a yellow sphere. (C) Descriptors for each enzyme/ligand were regressed against the experimentally determined selectivities, resulting in statistical models that enabled mechanistic insights and predicted the outcomes of out-of-sample substrates and mutants.

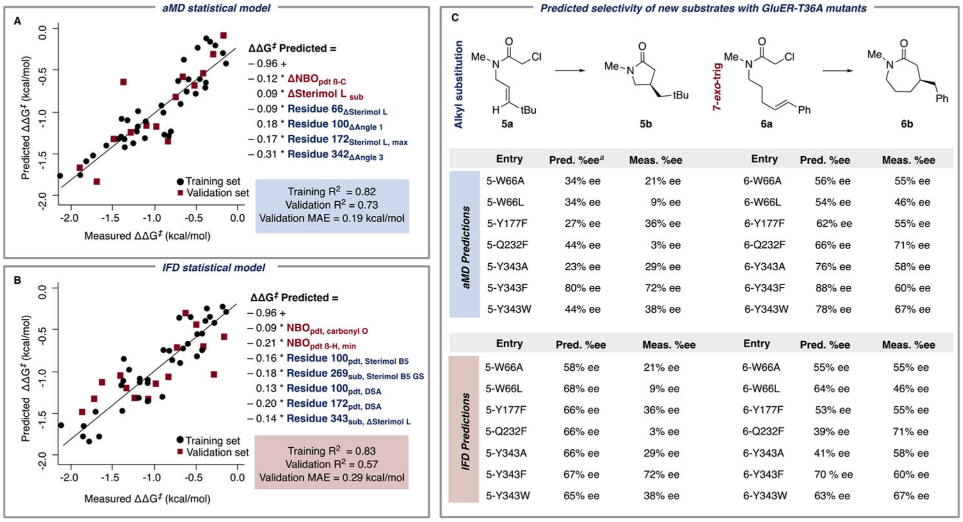

	Entry	Pred. %ee[a]	Meas. %ee	Entry	Pred. %ee	Meas. %ee
aMD Predictions	5-W66A	34% ee	21% ee	6-W66A	56% ee	55% ee
	5-W66L	34% ee	9% ee	6-W66L	54% ee	46% ee
	5-Y177F	27% ee	36% ee	6-Y177F	62% ee	55% ee
	5-Q232F	44% ee	3% ee	6-Q232F	66% ee	71% ee
	5-Y343A	23% ee	29% ee	6-Y343A	76% ee	58% ee
	5-Y343F	80% ee	72% ee	6-Y343F	88% ee	60% ee
	5-Y343W	44% ee	38% ee	6-Y343W	78% ee	67% ee

	Entry	Pred. %ee	Meas. %ee	Entry	Pred. %ee	Meas. %ee
IFD Predictions	5-W66A	58% ee	21% ee	6-W66A	55% ee	55% ee
	5-W66L	68% ee	9% ee	6-W66L	64% ee	46% ee
	5-Y177F	66% ee	36% ee	6-Y177F	53% ee	55% ee
	5-Q232F	66% ee	3% ee	6-Q232F	39% ee	71% ee
	5-Y343A	66% ee	29% ee	6-Y343A	41% ee	58% ee
	5-Y343F	67% ee	72% ee	6-Y343F	70 % ee	60% ee
	5-Y343W	65% ee	38% ee	6-Y343W	63% ee	67% ee

Figure 2.

aMD and IFD statistical models with ligand descriptors (red) and enzyme descriptors (blue). (A) The aMD model had a training and validation R^2 of 0.82 and 0.73, respectively, a leave-one-out (LOO) R^2 of 0.70, and a 4-fold R^2 of 0.67. (B) The IFD model had a training and validation R^2 of 0.83 and 0.57, respectively, LOO R^2 of 0.73, and a 4-fold R^2 of 0.70. (C). Enantioselectivities of reactions with **5a** and **6a** to form **5b** and **6b**, respectively, predicted from the aMD and IFD models. [a]Predicted from aMD model 2, Figure S3.

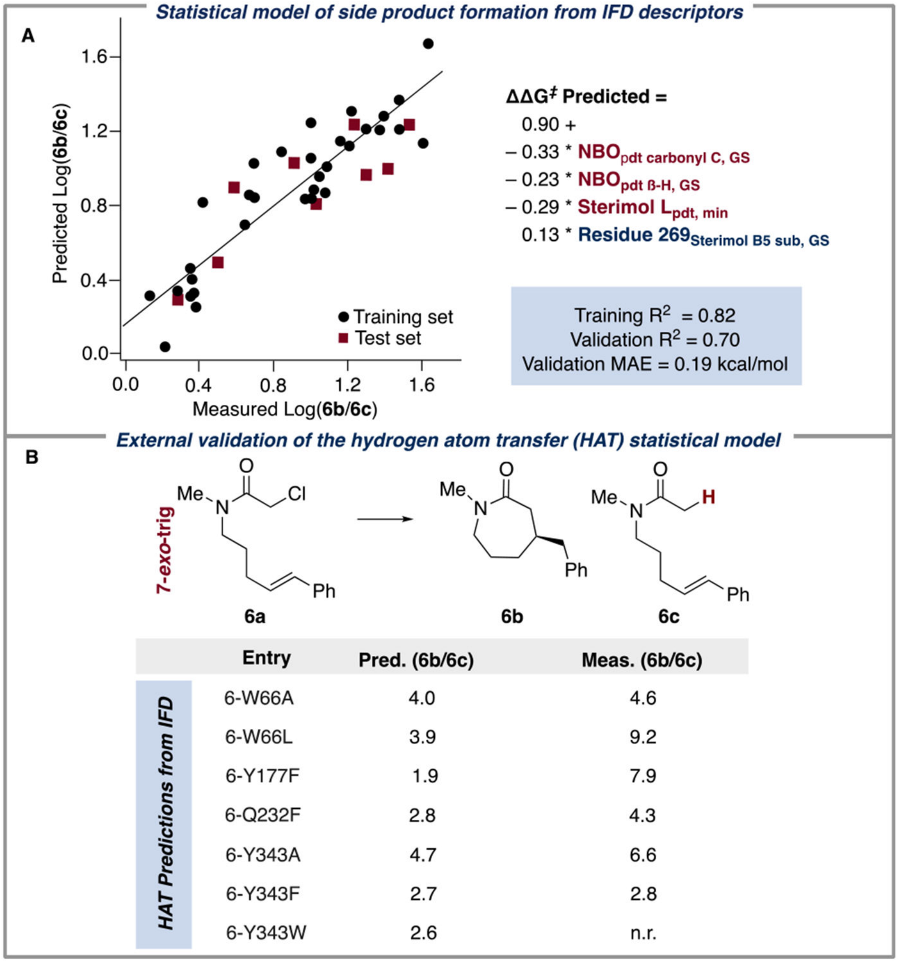

Entry	Pred. (6b/6c)	Meas. (6b/6c)
6-W66A	4.0	4.6
6-W66L	3.9	9.2
6-Y177F	1.9	7.9
6-Q232F	2.8	4.3
6-Y343A	4.7	6.6
6-Y343F	2.7	2.8
6-Y343W	2.6	n.r.

Figure 3.

Statistical model of HAT side product formation. (A) Regressing experimental ratios of cyclization: HAT with the IFD descriptor set resulted in the best statistical model (training and validation R^2 of 0.82 and 0.70, respectively, LOO R^2 of 0.76, and a 4-fold R^2 of 0.70). The model had three ligand descriptors (red) and one enzyme descriptor (blue). (B) HAT model predictions on substrate **6a**.

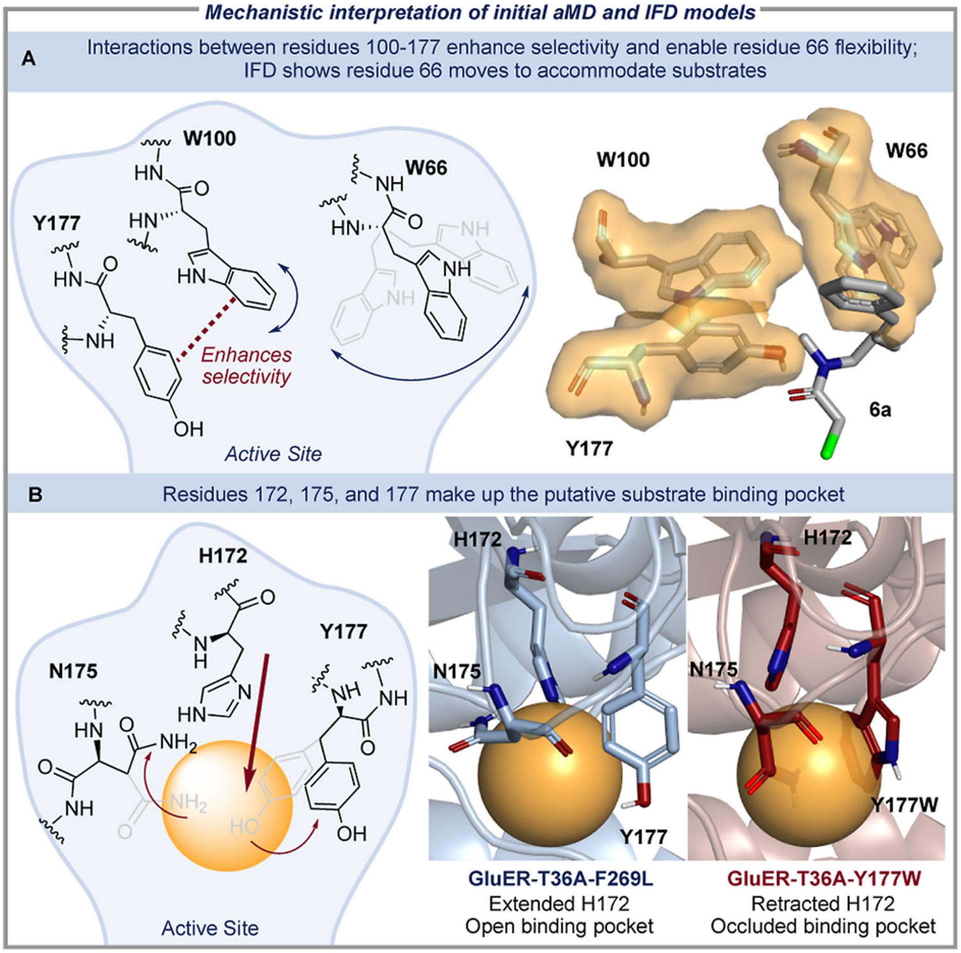
Mechanistic interpretation of initial aMD and IFD models
A
Interactions between residues 100-177 enhance selectivity and enable residue 66 flexibility; IFD shows residue 66 moves to accommodate substrates
W100
Y177
W66
HN
O
HN
NH
Enhances selectivity
OH
Active Site
W100
W66
Y177
6a
B
Residues 172, 175, and 177 make up the putative substrate binding pocket
H172
N175
Y177
NH₂
HO
OH
Active Site
H172
N175
Y177
H172
N175
Y177W
GluER-T36A-F269L
Extended H172
Open binding pocket
GluER-T36A-Y177W
Retracted H172
Occluded binding pocket

Figure 4.

Mechanistic interpretation of descriptors from initial models. (A) The aMD conformers demonstrated that when aromatic residues 100 and 177 were closely associated, interactions between residues 66 and 100 were precluded, inducing residue 66 flexibility and higher selectivity. The IFD conformational ensembles (right) corroborated that the flexibility of residue 66 is necessary for substrate binding. (B) The term Residue $172_{\mathrm{Sterimol}\ L,\mathrm{max}}$ from the aMD model indicated that extended configurations of H172 facilitated selectivity. Examination of enzyme conformers where this term was large (GluER-T36A-F269L = 6.7 Å) showed H172 to be extended (blue) and revealed an open binding pocket (yellow sphere); this binding pocket was occluded in structures where values of this parameter were small (GluER-T36A-Y177W = 5.2 Å, red).

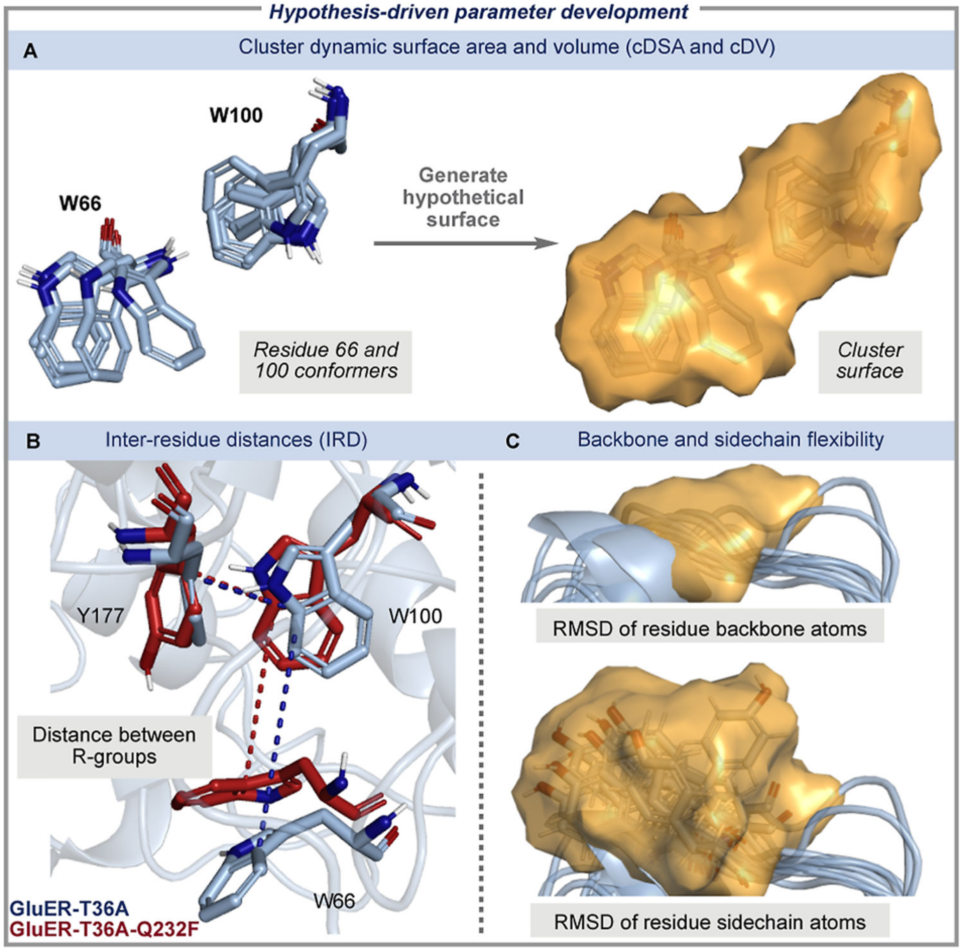
Hypothesis-driven parameter development
A
Cluster dynamic surface area and volume (cDSA and cDV)
W100
W66
Generate hypothetical surface
Residue 66 and 100 conformers
Cluster surface
B
Inter-residue distances (IRD)
Y177
W100
Distance between R-groups
W66
GluER-T36A
GluER-T36A-Q232F
C
Backbone and sidechain flexibility
RMSD of residue backbone atoms
RMSD of residue sidechain atoms

Figure 5.

Hypothesis-driven parameter development. (A) Cluster DSAs and (B) IRD were measured to explicitly describe the interactions between residues 66/100/177 and 172/175/177. (C) The overall residue flexibility was measured by computing the RMSD of residue backbone and side-chain atoms.

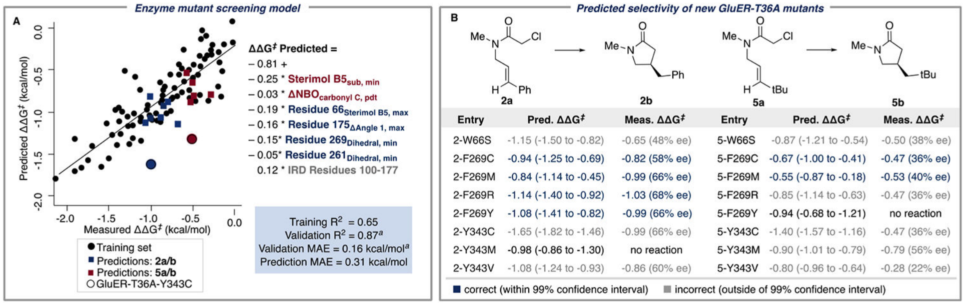

Entry	Pred. ΔΔG‡	Meas. ΔΔG‡	Entry	Pred. ΔΔG‡	Meas. ΔΔG‡
2-W66S	-1.15 (-1.50 to -0.82)	-0.65 (48% ee)	5-W66S	-0.87 (-1.21 to -0.54)	-0.50 (38% ee)
2-F269C	-0.94 (-1.25 to -0.69)	-0.82 (58% ee)	5-F269C	-0.67 (-1.00 to -0.41)	-0.47 (36% ee)
2-F269M	-0.84 (-1.14 to -0.45)	-0.99 (66% ee)	5-F269M	-0.55 (-0.87 to -0.18)	-0.53 (40% ee)
2-F269R	-1.14 (-1.40 to -0.92)	-1.03 (68% ee)	5-F269R	-0.85 (-1.14 to -0.63)	-0.47 (36% ee)
2-F269Y	-1.08 (-1.41 to -0.82)	-0.99 (66% ee)	5-F269Y	-0.94 (-0.68 to -1.21)	no reaction
2-Y343C	-1.65 (-1.82 to -1.46)	-0.99 (66% ee)	5-Y343C	-1.40 (-1.57 to -1.16)	-0.47 (36% ee)
2-Y343M	-0.98 (-0.86 to -1.30)	no reaction	5-Y343M	-0.90 (-1.01 to -0.79)	-0.79 (56% ee)
2-Y343V	-1.08 (-1.24 to -0.93)	-0.86 (60% ee)	5-Y343V	-0.80 (-0.96 to -0.64)	-0.28 (22% ee)

■ correct (within 99% confidence interval) ■ incorrect (outside of 99% confidence interval)

Figure 6.

Updated model enabled virtual screening and prediction of the selectivity of new GluER-T36A mutants. (A) Similar to the initial models, the updated statistical model has two ligand descriptors (red), several residue-based enzyme descriptors (blue), and one IRD parameter (gray) that measures the distance between residues 100 and 177. (B) Predicted enantioselectivities of **2a** and **5a** with untested GluER-T36A variants; the range for the predictions was computed at a 99% confidence interval using bootstrap subsampling. [a]Training and validation set statistics were computed with a 70:30 split, as further described in the Supporting Information.

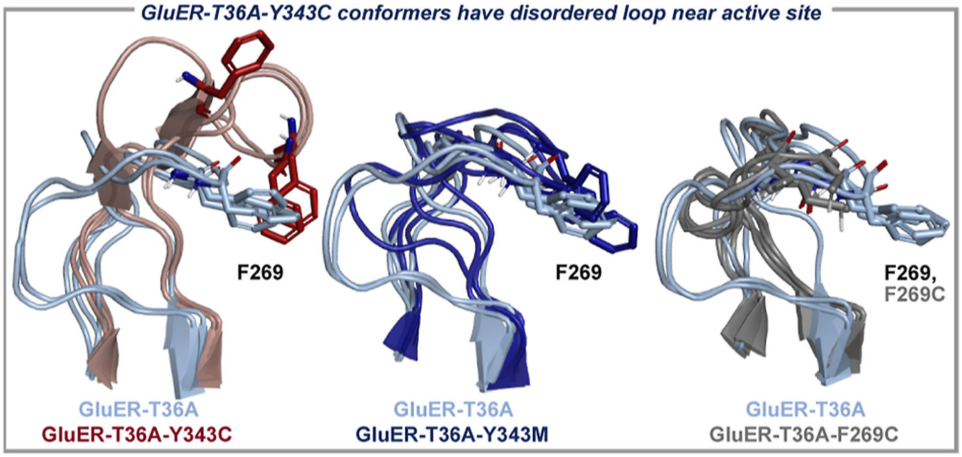

Figure 7.

GluER-T36A-Y343C is structurally unique. The aMD conformational ensemble of GluER-T36A-Y343C (red) displays disorder in the 269-loop region compared to GluER-T36A (light blue). Other variants such as GluER-T36A-Y343M (dark blue) and GluER-T36A-F269C (gray) maintain structures similar to GluER-T36A.

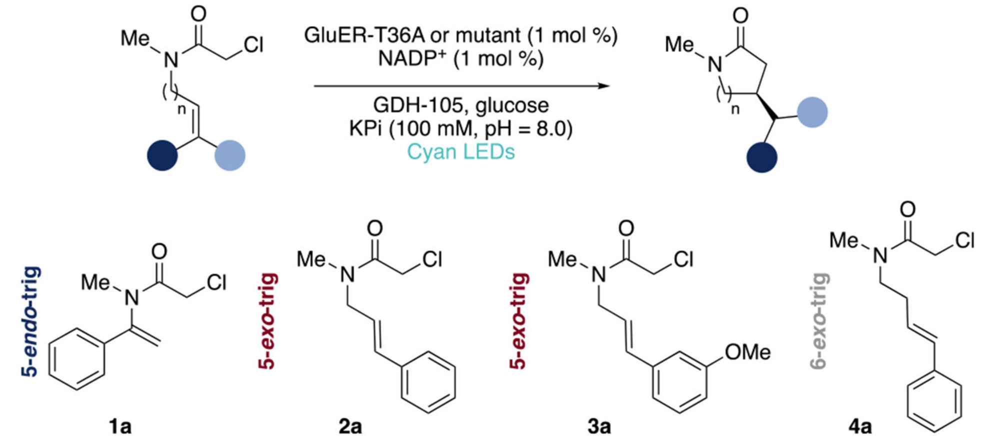

Scheme 1.

Enantioselective Cyclization Catalyzed by GluER-T36A and Mutants